remote sensing

MDPI

Article

Historical Hazard Assessment of Climate and Land Use–Land Cover Effects on Soil Erosion Using Remote Sensing: Case Study of Oman

Shahab Aldin Shojaeezadeh [1,2], Malik Al-Wardy [2,3,*], Mohammad Reza Nikoo [4], Mehrdad Ghorbani Mooselu [5], Nasser Talebbeydokhti [6], Nasrin Alamdari [7] and Amir H. Gandomi [8,9]

1 Section of Soil Science, Faculty of Organic Agricultural Sciences, University of Kassel, 37213 Witzenhausen, Germany; shahab2710@gmail.com
2 Center for Environmental Studies and Research, Sultan Qaboos University, Muscat 123, Oman
3 Department of Soils, Water, and Agricultural Engineering, Sultan Qaboos University, Muscat 123, Oman
4 Department of Civil and Architectural Engineering, Sultan Qaboos University, Muscat 123, Oman
5 Norwegian Institute for Sustainability Research (NORSUS), 1672 Fredrikstad, Norway
6 Department of Civil and Environmental Engineering, Shiraz University, Shiraz 71946, Iran
7 Department of Civil and Environmental Engineering, Resilient Infrastructure and Disaster Response (RIDER) Center, Florida A&M University-Florida State University College of Engineering, Tallahassee, FL 32310, USA
8 Faculty of Engineering and Information Technology, University of Technology Sydney, Ultimo, NSW 2007, Australia
9 University Research and Innovation Center (EKIK), Óbuda University, 1034 Budapest, Hungary
* Correspondence: mwardy@squ.edu.om

Abstract: Human activities, climate change, and land-use alterations accelerated soil erosion in recent decades and imposed significant threats to soil fertility and stability worldwide. Understanding and quantifying the spatiotemporal variation of soil erosion risks is crucial for adopting the best management practices for surface soils conservation. Here, we present a novel high-resolution (30 m) soil erosion framework based on the G2 erosion model by integrating satellite and reanalysis datasets and Machine Learning (ML) models to assess soil erosion risks and hazards spatiotemporally. The proposed method reflects the impacts of climate change in 1 h time resolutions and land use in 30 m scales on soil erosion risks for almost 4 decades (between 1985 and 2017). The soil erosion hazardous maps were generated/evaluated using Extreme Value Analysis (EVA), utilizing long-term annual soil erosion estimations/projections to aid policymakers in developing management strategies to protect lands against extreme erosion. The proposed framework is evaluated in the Sultanate of Oman, which lacks soil erosion estimation/assessment studies due to data scarcity. Results indicate that soil erosion has increasing perilous trends in high altitudes of the Sultanate of Oman that may cause substantial risks to soil health and stability.

Keywords: soil erosion; remote sensing; empirical orthogonal function; extreme value analysis; G2 model

Citation: Shojaeezadeh, S.A.; Al-Wardy, M.; Nikoo, M.R.; Mooselu, M.G.; Talebbeydokhti, N.; Alamdari, N.; Gandomi, A.H. Historical Hazard Assessment of Climate and Land Use–Land Cover Effects on Soil Erosion Using Remote Sensing: Case Study of Oman. *Remote Sens.* **2024**, *16*, 2976. https://doi.org/10.3390/rs16162976

Academic Editor: Xihua Yang

Received: 16 May 2024
Revised: 5 August 2024
Accepted: 7 August 2024
Published: 14 August 2024

1. Introduction

Accelerated soil erosion poses a significant risk to soil health, the ecological environment, and socio-economic development, as it can lead to soil degradation [1–3]. In arid/semi-arid regions, soil erosion significantly contributes to desertification [4–6], and is primarily driven by human activities and climate change, according to the United Nations Convention to Combat Desertification [7–10]. Thus, it is of utmost importance to study the soil erosion characteristics influenced by climate change and land cover shifts in marginal environments such as arid/semi-arid regions [11–15]. Therefore, quantification of soil erosion toward sustainable developments is a prerequisite [16–18]. Soil erosion models are efficacious tools to predict soil loss and its risks [19–21]. The Revised Universal Soil

Loss Equation (RUSLE) is widely accepted and has recently been combined with GIS to extend soil erosion estimation in large-scale modeling [5,22–24]. Recent advances in cloud computing, satellite data, and model integration with GIS capabilities set an opportunity to adjust the traditional RUSLE equation to predict soil erosion variability at different spatial and temporal scales [24]. The G2 erosion model is a modified version of the RUSLE equation, which shares the power of remote sensing methods on soil erosion modeling with the capability to integrate with cloud computing platforms such as Google Earth Engine (GEE) to assess soil erosion hazards spatiotemporally.

Soil erosion varies through time and space, either by climate change or land-use shifts [23,25,26]. Studies have shown that, due to recent climate change, soil erosion hazards could also change in the future [22,27,28]; however, most studies have ignored spatiotemporal variations of soil erosion on hazard assessment [29–32]. For example, factor parameterization of the RUSLE [23,33,34], soil erosion vulnerability maps based on severity classification [25,35,36], soil erosion hazard indexes [37–40], and decision-making approaches by integrating threats to human life and environmental habitats [41–44] are stationary approaches to assessing soil erosion hazards. Although soil erosion hazard assessment based on climate change and socio-economic scenarios has forecasted soil erosion hazards [23,45–47], a practical method to identify soil erosion hazards based on historical events and nonstationary assumptions on time is rarely proposed.

Recent advancements in cloud-backed environmental and satellite imagery databases and computing platforms such as GEE have allowed soil erosion models to predict soil erosion at various scales and times [48–51]. The ability of remote sensing and GIS to retrieve ground information and handle large spatial data can help to model soil erosion over time and space, contributing to estimating various factors impacting soil erosion, including climate, vegetation cover, and slope length and steepness of soil erosion models [52–58]. However, most of the studies assumed the hypothesis, such as ignoring temporal variations, fixing management factors on land use classes, and disregarding bare lands with sand dunes and active dunes from estimation, which oversimplified the problem and restricted previous methods to calibrated regions.

This research proposed a feasible framework that uses the G2 erosion model (modified RUSLE) to estimate the spatiotemporal variation of soil erosion between 1985 and 2017 and identify soil erosion hazards for various return periods in the Sultanate of Oman. A variety of datasets, models, and methods were integrated into a framework to estimate G2 factors over time and space. Rainfall erosivity, sustainability, soil erodibility, and terrain influence factors were estimated utilizing remote sensing techniques and satellite imagery of Sentinel 2 and Landsat 5, 7, and 8 in the GEE platform. To assess soil erosion hazard, extreme value theory was used to investigate the spatiotemporal variation of soil erosion and prepare soil erosion hazard maps in various return periods (i.e., 5, 10, 25, 50 years). The proposed method can serve as a guideline to identify areas with high soil erosion rates and assist policymakers in developing land management strategies to protect lands against degradation and mitigate soil erosion hazards based on the likelihood and frequency of historical trends.

2. Materials and Methods

2.1. Soil Erosion Modeling and Limitations

Soil erosion modeling is extremely challenging. As a result, numerous methods have been developed to estimate soil erosion, such as the Universal Soil Loss Equation (USLE), initially introduced by [59] as follows:

$$A = R \times K \times LS \times C \times P \quad (1)$$

where A: *soilerosion* $\left(\mathrm{Mgha^{-1}yr^{-1}}\right)$, R: rainfall erosivity ($\mathrm{MJmmha^{-1}h^{-1}yr^{-1}}$), K: soil erodibility ($\mathrm{MghahMJ^{-1}ha^{-1}mm^{-1}}$), LS: slope length and steepness (dimensionless), C: cover management (dimensionless), and P: support practice (dimensionless) account for

different aspects of the soil erosion process [60]. However, Ref. [24] relooked at the USLE equation, modified factors as follows, and named it the G2 module:

$$A = \frac{R}{V} \times K \times \frac{LS}{L} \quad (2)$$

where the erosion-inducing factors of R: rainfall erosivity, K: soil erodibility, and LS: terrain influence are introduced as numerator factors and erosion-controlling factors of $V = \frac{1}{C}$: vegetation retention, and $L = \frac{1}{P}$: landscape effects are introduced as dominator factors. Erosion-inducing factors express natural erosion forces inherited from the Revised USLE (RUSLE), while erosion-controlling factors of vegetation retention (V) and landscape effect (L) express natural or human-induced anti-erosion factors, where $V \times L \geq 1$ can be seen as a sustainability factor. Two factors of R as a cumulative effect of rainfall erosive effects and S as a protective role of vegetation cover or land management are dynamic through time, while K and LS are static. Here, we proposed a novel methodology to estimate annual soil erosion between 1985 and 2017 (Figure 1).

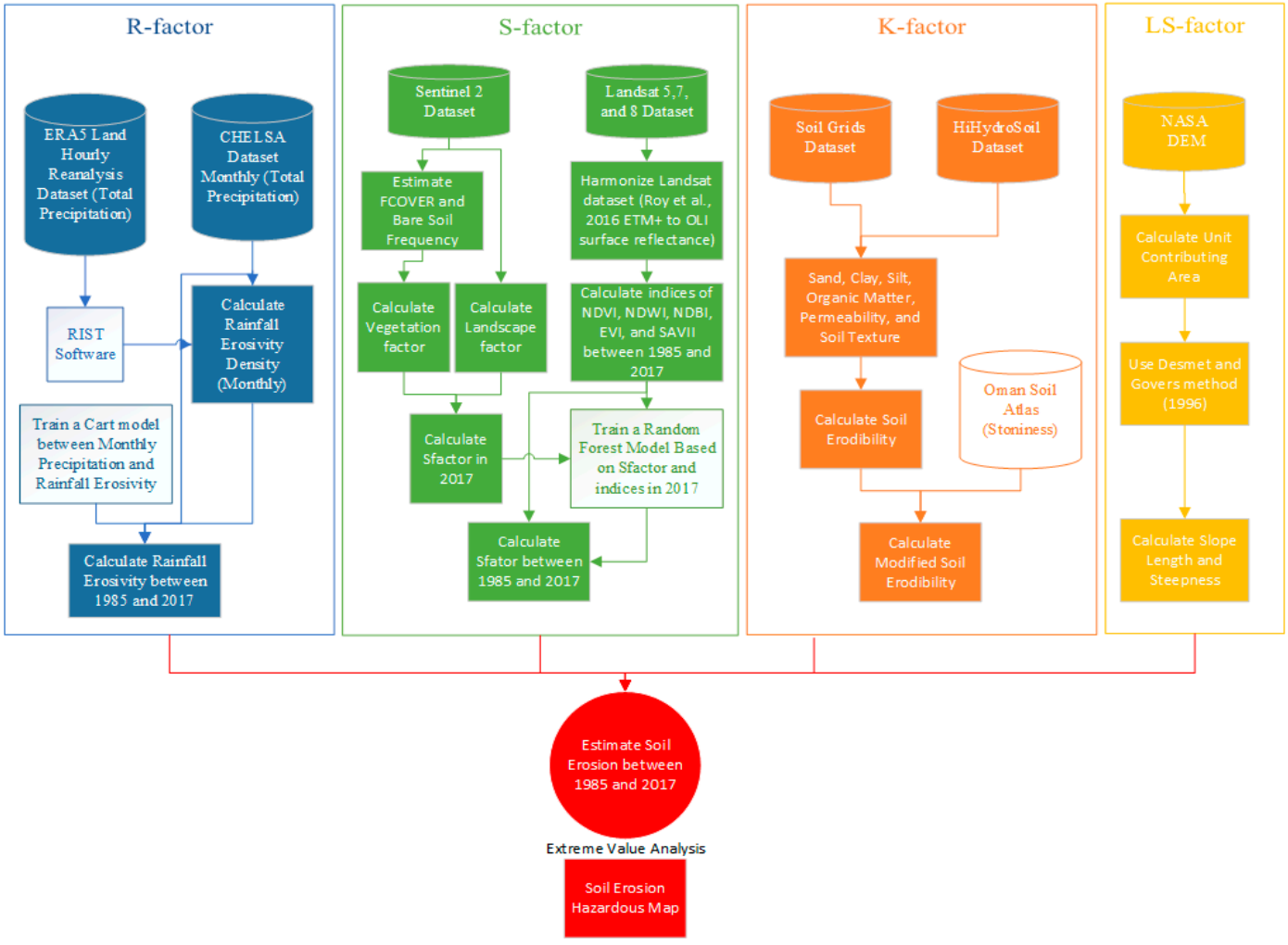

Figure 1. Flowchart of the proposed methodology [61].

The G2 erosion model is based on the RUSLE model that estimates soil erosion; it includes sheet and rill erosion processes but excludes gully and alluvial erosion processes. However, it remains the best available method to estimate soil erosion and, when combined with sediment yield equations (models), can estimate sediment transport [31,60,62]. Although we used the finest resolution dataset available for Oman, uncertainties in satellite data, the European Centre for Medium-Range Weather Forecasts Reanalysis 5th Generation

(ERA5) model, soil database accuracy, and elevation dataset precision led to uncertainties not associated with our methodology but related to the data itself. The G2 model inherited RUSLE limitations in terms of sheet and rill erosion including (1) no degradation modeling; (2) no alluvial modeling; (3) ignores gully erosion; (4) the rainfall erosivity factor is defined and measured based only on eastern regions of the United States, and (5) steep slopes have some extreme LS-factor values that cannot be resolved by any method, although some equations try to relax these factors [63]. Notably, the G2 model is very complex, implying a method designed for regional to continental scales (applicable worldwide) that eliminates the inability of the RUSLE equation in desert lands, in terms of data scarcity of vegetation retention and landscape effects.

2.2. Soil Erosion Factors

2.2.1. Rainfall Erosivity Factor (R)

Ref. [64] expresses the potential of rainfall energy to detach soil particles and the capacity to transport soil within a specific time period (erosive events). Experimental research [65] that related rainfall characteristics to plot-years of thousands of rainfall and runoff data is summarized in the following equation:

$$EI_{30} = I_{30} \sum_{i=1}^{N} e_i v_i \quad (3)$$

where EI_{30} is the mean annual erosivity index, which is the multiplication of I_{30} as the maximum intensity in 30-min intervals (mmha^{-1}), and summation of the multiplication of e_i as the rainfall energy per surface unit and rainfall volume of an erosive event (MJmm^{-1}ha^{-1}), and v_i is the rainfall volume during erosive events (mm) in each erosive event (i). In different versions of USLE, RUSLE, and RUSLE2, various methods have been proposed to estimate rainfall energy (e) based on [66,67] the following equation:

$$e = e_m[1 - aexp(-bI_i)] \quad (4)$$

where e_m is the maximum unit energy, which is estimated to be 0.29 by [68], a and b are empirical coefficients that are different in various versions, and I_i is the rainfall intensity in each erosive event. The most recent version of RUSLE2 proposed empirical coefficients as $a = 0.72$ and $b = -0.082$ to estimate rainfall energy [69].

After determining the rainfall erosivity for every single erosive event (Equations (3) and (4)), the average annual rainfall erosivity (MJmmha^{-1}h^{-1}yr^{-1}) is estimated by Equation (5):

$$R = \frac{\sum_{j=1}^{n} \sum_{m=1}^{k_j} EI_{30_m}}{n} \quad (5)$$

where n is the number of years; k_j is the number of events in year j; and m is the index of every single erosive event and corresponding rainfall erosivity.

RUSLE2 also proposed an erosivity density index for calculating rainfall erosivity in the United States, which has various advantages, including better estimation of erosivity, better performances in mountain areas, and the capability to use shorter-than-10-year rainfall records [69]. We calculated the monthly erosivity density by using Rainfall Intensity Summarization Tool (RIST) software (Version 3.6) [70] on 60 min intervals of total precipitation and employing the ERA5 Land Hourly Reanalysis dataset [71] on the Sultanate between 1985 and 2017. Then, rainfall erosivity density was multiplied by the average monthly precipitation of Climatologies at high resolution for the earth's land surface areas (CHELSA V2) dataset (rooted in ERA5 reanalysis dataset) [72] each month to calculate monthly rainfall erosivity and at last, calculate annual rainfall erosivity between 1985 and 2017, adding monthly rainfall erosivity on each year. Finally, the rainfall erosivity maps were interpolated using the Cart Machine Learning (ML) model in 1 km resolution,

employing monthly precipitation of the CHELSA V2 dataset as a covariate and estimated rainfall erosivity in the grid cells of the ERA5 Land Hourly dataset in 11 km resolution [73].

2.2.2. Vegetation Retention Factor (V)

The cover management spin-off in the RUSLE equation is the vegetation retention factor, which is a more logical way of looking at natural or agricultural vegetation's effect on soil protection from erosion. This factor identifies three types of effects: (1) the canopy effect (also suggested to be considered in cover management of the RUSLE2 equation as the effect of crown density and closure degree above the surface) [24], (2) the small plants and residues effect as natural protection on the surface [74], and (3) organic matter and soil structure enhancement under the surface, which can express the effect of crop rotations on erosion.

Vegetation retention is the erosion-controlling factor determining whether or not vegetation is present on croplands or grasslands over time to protect soil from erosion. It can be estimated by the following equation [24]:

$$V_m = exp\left[10 \times \left(1 - BS_f\right) \times Fcover_m\right] \quad (6)$$

where V_m is the composite of the monthly vegetation retention factor, BS_f is the bare soil frequency where $1 - BS_f$ expresses the vegetation cover frequency, $Fcover_m$ is the composite of monthly green vegetation cover fraction, and m determines the month of calculation. The annual vegetation retention factor is the summation of monthly vegetation retention in the monitoring period (n):

$$V = \frac{\sum_{i=1}^{n} V_{m,i}}{n} \quad (7)$$

where V is annual vegetation retention. We used the Google Earth Engine (GEE) platform to estimate $Fcover_m$ employing Sentinelhub custom scripts (https://github.com/sentinel-hub/custom-scripts/tree/master/sentinel-2/fcover (accessed on 10 March 2021)) and BS_f employing the Geospatial Soil Sensing System (GEOS3) algorithm (estimated by Normalized Vegetation index (NDVI) and Normalized Burn ratio 2 (NBR2)) using Sentinel-2 imagery data.

2.2.3. Landscape Effect (L)

As expressed in the RUSLE equation, the practice management factor incorporates the effect of various erosion-controlling landscape features that interrupt the effect of rainfall–runoff on water motion, such as tillage practices. Ref. [24] proposed a formula to estimate this factor using a 3 × 3 Sobel filter (an edge-detection filter) applied to the Near-Infrared (NIR) band of Sentinel 2 as follows:

$$L = 1 + \sqrt{\frac{s_f}{DN_{max}}} \quad (8)$$

where L is the landscape effect (dimensionless), s_f is the Sobel filter value (dimensionless), and DN_{max} is the maximum potential reflectance value (which is 10,000 in Sentinel 2 data on GEE).

2.2.4. Sustainability Factor ($S = \frac{1}{V \times L}$)

The sustainability factor expresses how much vegetation and practices can protect soil from erosion. We used Sentinel 2 data in 2017 to estimate this factor in the GEE platform. However, to estimate the effect of sustainability factors between 1985 and 2017, Sentinel 2 data is not available before 2015. Therefore, to overcome this limitation, we developed a Machine Learning (ML) regression model based on various indices estimated by Landsat 5, 7, and 8 imageries. First, we harmonized the Landsat 5, 7, and 8 surface reflectances

to translate Enhanced Thematic Mapper Plus (ETM+) sensor values to the Operational Land Imager (OLI) sensor values using [61] proposed equation in GEE. Then, harmonized Landsat data were used to estimate various annual vegetation, built-up area, and water extent indices as covariate parameters of an ML Random Forest (RF) regression model and correlate these parameters with the calculated sustainability factor in 2017. We used annual NDVI, Normalized Difference Water Index (NDWI), Normalized Difference Built-up Index (NDBI), Normalized Ration Vegetation Index (NRVI), Enhanced Vegetation Index (EVI), and Soil-Adjusted Vegetation Index (SAVI) indices to train the RF regression model and project sustainability factor between 1985 and 2017. Each index has been applied to reflect various effects of land use and land cover changes over time. The NDVI indices imitate the density of green on a patch of land, NDWI expresses the plant water content, NDBI mitigates the effect of terrain elucidation and atmospheric effects on vegetation, NRVI distinguishes vegetation from the soil, EVI corrects some atmospheric conditions and background noises in canopy cover, and SAVI adjusts the effect of soil brightness on NDVI where vegetation cover is low. Therefore, various indices reflect different aspects of vegetation features on sustainability factor projection for the time between 1985 and 2017.

The upscaling of the sustainability factor estimated by Sentinel 2 from 10 m to Landsat composites of 30 m may eliminate the landscape effect. Our analysis shows the effect of this change on the average, median, and maximum. The variance of the sustainability factor is lower than 0.1%, but the minimum values are overestimated from 0.002 to 0.24. Further analysis revealed the pixels with values lower than 0.24 are rare (380 pixels out of 3 billion), which is lower than the value that could change results tremendously.

2.2.5. Soil Erodibility Factor (K)

Soil erodibility (K-factor) is the soil's inherent susceptibility to erosion. The K-factor, defined by soil properties such as permeability, texture, structure, and organic matter content, represents the soil's reaction to detachment and transport by raindrops and surface flow as a mean annual value. Ref. [34] proposed an equation to relate organic matter, texture, permeability, sand, clay, and silt content of the soil profile to *K*-factor, as follows:

$$K = \left[\left(2.1 \times 10^{-4} M^{1.14}(12 - OM) + 3.25(s - 2) + 2.5(p - 3)/100\right)\right] \times 0.1317 \quad (9)$$

where M is the textural factor and defined as $M = (m_{silt} + m_{sand})(100 - m_c)$, in which m_c is the percent of clay, m_{sand} is the percent of sand, and m_{silt} is the percent of silt. Also, OM indicates the percent of organic matter; s is the soil class structure, and p represents the permeability class.

To estimate soil erodibility, various datasets available through the GEE platform have been used. The SoilGrids dataset at 250 m of geospatial resolutions has been used to derive clay, sand, silt, and organic matter (scaling soil organic carbon to soil organic matter using a 1.72 factor as suggested by [75]) on the average of the first three layers with depths range between 0–30 cm [76]. The bulk density was used to estimate the packing density of the soil to reflect the effect of subsoil compactness in texture classification [77]. The influence of organic matter on soil texture [78] (specifically for cases where organic matter is 20% with 0% clay and 30% with 50% clay) is considered to determine soil structure classes at a 250 m resolution [79]. To calculate permeability classes, the hydrologic group of soil and saturated hydraulic conductivity from the HiHydroSoil v2 dataset are used [80]. Volumetric fractions of coarse fragments from the SoilGrids dataset are employed to modify saturated hydraulic conductivity to eliminate the effect of rock fragments (stoniness) on soil erodibility estimation [80,81].

2.2.6. Slope Length and Steepness Factor (LS)

The combined slope length and steepness factor (LS-factor) describe the effect of topography's shape on soil erosion. The existing methods for assessing the impact of terrain on soil erosion struggle with complex landscapes like steep slopes or short slope

lengths. This study addresses this by employing the unit-contributing area concept to calculate slope length and steepness. This method breaks the slope down into smaller, more manageable segments, resulting in a more consistent representation of slope steepness. This approach is effective across diverse terrains, from steep mountains to flat plains. The unit-contributing area concept and the original equation proposed by [82] were used to derive the LS-factor as follows:

$$\begin{cases} S = 10.8 \times sin(\theta) + 0.03, slope < 9\% \\ S = 16.8 \times sin(\theta) - 0.05, slope \geq 9\% \end{cases}$$
$$L_{i,j} = \frac{\left(A_{i,j}+D^2\right)^{m+1} - A_{i,j-in}{}^{m+1}}{D^{m+2} \times x_{i,j}^{m} \times 22.13^{m}} \quad (10)$$
$$m = \frac{\beta}{\beta+1}$$
$$\beta = \frac{\frac{sin(\theta)}{0.0896}}{0.56+3\times[sin(\theta)]^{0.8}}$$

where S is the slope steepness, θ is the gradient of the slope in degrees, $L_{i,j}$ is the slope length, $A_{i,j}$ is the upstream contributing area at the inlet of the grid cell (i,j) (m^2), D is the grid cell size (m), $x_{i,j} = sin(a_{i,j}) + cos(a_{i,j})$, $a_{i,j}$ is the aspect direction of the grid cell (i,j), and β is the ratio of rill to inter-rill erosion. To estimate the LS-factor, we used System for Automated Geoscientific Analyses (SAGA) GIS software and the National Aeronautics and Space Administration Digital Elevation Model (NASADEM, the void-filled SRTM data) in 30 m resolution, because the lower resolution (>30 m) would lead to an overestimation of the topography effect on soil erosion.

2.3. Extreme Value Analysis (EVA)

Extreme value analysis (EVA) is a risk-based statistical analysis that assesses the magnitude and frequency of hazardous events [83] and evaluates the likelihood of extreme values based on a few basic assumptions (e.g., the statistical distribution of extremes) and observed/measured data. EVA is a classical frequency analysis that refers to the study of events' probability. It is often utilized in regulatory situations to determine design values for infrastructures and can be used to estimate extreme values for different return periods (return interval, recurrence interval, or repetition interval). To analyze the maxima of historical observations, the Generalized Extreme Value (GEV) distribution is usually applied. GEV developed in extreme value theory to combine the Gumbel, Fréchet, and Weibull extreme value distributions [84] with a probability density function (PDF) as follows:

$$F(x) = exp\left[-(1+\frac{\gamma(x-\mu)}{\alpha})^{-1/\gamma}\right] \quad (11)$$

where $\alpha > 0$ is the scale parameter, $\mu \epsilon R$ is the location parameter, and $\gamma \epsilon R$ is the location parameter, when $\gamma \neq 0$. If $\gamma = 0$, the GEV distribution will be the Gumbel distribution:

$$F(x) = exp\left[-exp(\frac{(x-\mu)}{\alpha})\right] \quad (12)$$

The fit to estimate the GEV parameters can be done by various proposed methods [85]. In this study, we used the Maximum Likelihood (ML) algorithm [86] to estimate scale, location, and shape parameters and the Block Maxima approach at the annual frequency to extract maximum values. Then, based on fitted GEV distribution, soil erosion hazards are estimated/projected for specific return intervals (i.e., 5, 10, 25, and 50 years).

2.4. Compare ERA5 and Ground-Based Observations

Two categorical statistical indices, the probability of detection (POD) and critical success index (CSI), were used to determine the detection accuracy of the ERA5 measurements compared to ground station observations (the Sultanate of Oman Meteorological Organization's hourly rainfall dataset). The POD describes the proportion of ground ob-

servations correctly identified by ERA5 estimates (Equation (13) with an optimum value of 1), while the CSI assesses the ERA5 products' ability to identify precipitation over an area (Equation (14) with an optimum value of 1). The bias (error) level in ERA5 products was then calculated using three classical statistical indices: mean absolute error (MAE), root mean square error (RMSE), and relative bias (RBIAS). MAE, in particular, provides a general evaluation of errors for ERA5 precipitation data against rain gauge observations (Equation (15) with an optimum value of 0); RMSE indicates the magnitude of the error (Equation (16) with an optimum value of 0), and RBIAS quantifies systematic errors between two precipitation datasets (Equation (17) with an optimum value of zero percent). Finally, the correlation coefficient (CC) index (Equation (18) with an optimum value of 1) was used to determine the consistency of the ERA5 products with ground observations. The statistical indices were calculated using the following formulas:

$$POD = \frac{N_{RS}}{N_{RS} + N_R} \tag{13}$$

$$CSI = \frac{N_{RS}}{N_{RS} + N_S + N_R} \tag{14}$$

$$MAE = \frac{1}{n}\sum_{i=1}^{n}|D_i - O_i| \tag{15}$$

$$RMSE = \sqrt{\frac{1}{n}\sum_{i=1}^{n}(D_i - O_i)^2} \tag{16}$$

$$RBIAS = \frac{\frac{1}{n}\sum_{i=1}^{n}(D_i - O_i)}{\sum_{i=1}^{n}(O_i)} \times 100 \tag{17}$$

$$CC = \frac{\sum_{i=1}^{n}\left(D_i - \overline{D}\right)\left(O_i - \overline{O}\right)}{\sqrt{\sum_{i=1}^{n}\left(D_i - \overline{D}\right)\sum_{i=1}^{n}\left(O_i - \overline{O}\right)}} \tag{18}$$

where n is the number of records; D_i is the value of rainfall detected by the model; O_i indicates the precipitation value observed by ground stations; $\overline{D}$ and $\overline{O}$ are mean values of D_i and O_i, respectively; N_{RS} is the number of observed and detected events by both the rain gauge and model; N_R is the number of events observed by a rain gauge but not detected by the model; and N_S specifies the number of events that are detected by the model but not observed by the rain gauge.

3. Results

The Sultanate of Oman is characterized by an arid/semi-arid climate, typically experiencing monsoons in the southern region shorelines, while the interior plateau is extremely hot and dry. The rainfall pattern in the northern regions from December to February and the southern regions during the monsoon season from mid-June until mid-September ranges from high intensity to extreme. While Oman is mainly covered by desert and active sand dunes, the higher altitudes of the northern mountains are covered mainly by scattered vegetation and shrubs, and the mountains in the southern region are covered with sparse forests (Figure 2). Further details are provided in the Environmental Settings (see Supplementary Materials, Figures S1–S4).

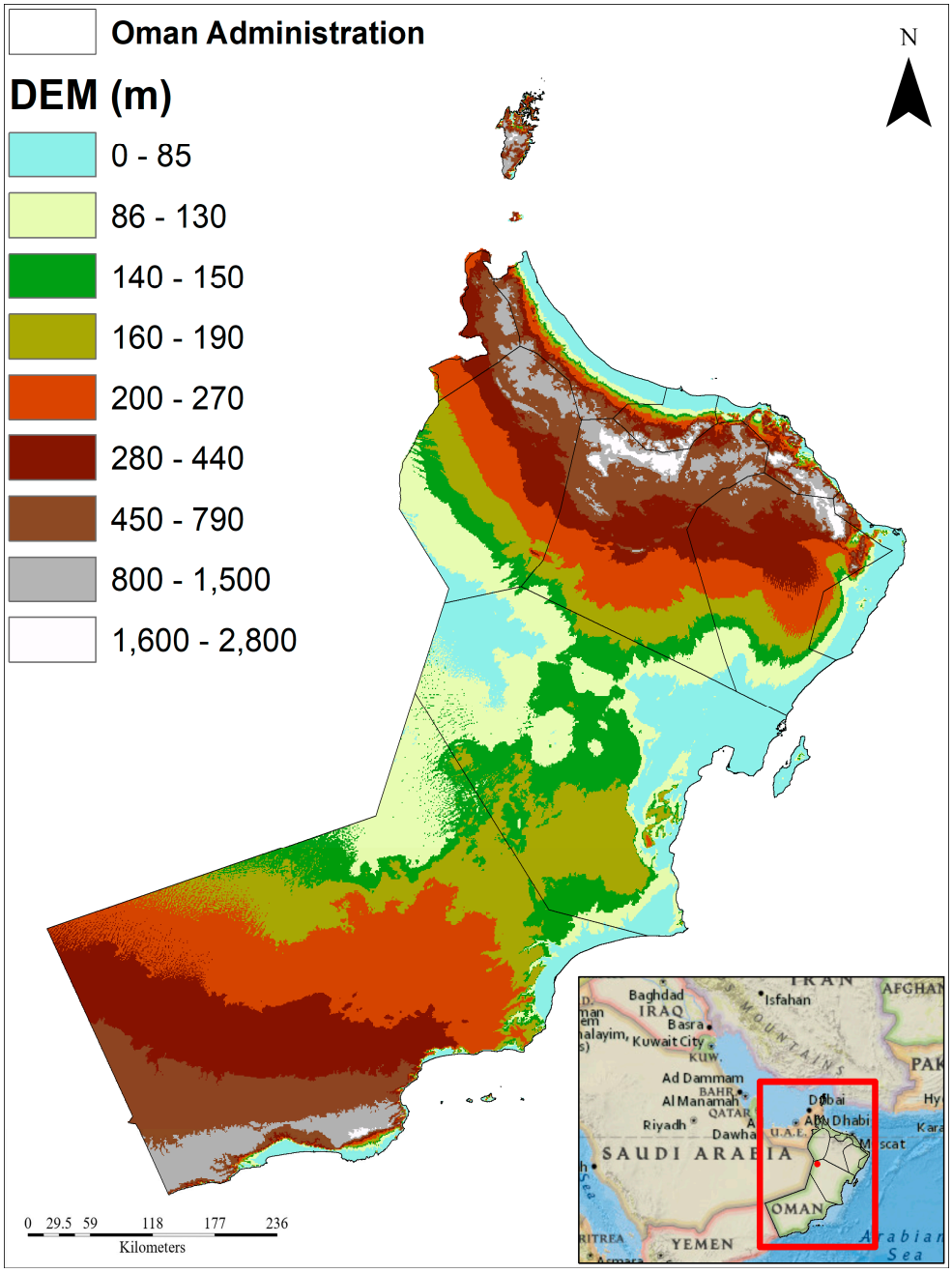

Figure 2. Case study area.

3.1. Rainfall Erosivity Factor

We estimated rainfall erosivity in the range from 1985 to 2017, and the Hovmöller diagram shows spatiotemporal variations (Figure 3A). Spatial variation of rainfall erosivity across Oman shows the highest rainfall erosivity occurs near shorelines, which are affected mainly by the monsoon rains from mid-June to mid-September named the Khareef effect. Temporal variation of rainfall erosivity indicates the specific years of 1983, 1996, 2002, and 2015 had the highest values, reaching 2400 (MJmmha^{-1}h^{-1}yr^{-1}) on average (Figure 3A,D). Additionally, analyzing the spatiotemporal variation of rainfall erosivity revealed the lowest values were related mostly to desert lands, where most of the year is dry, and the highest values to the high altitudes of the northern and southern mountains. Therefore, rainfall erosivity variation suggests that areas near shorelines and the top of the mountains are more susceptible to soil erosion caused by intense rainfall's energy drops.

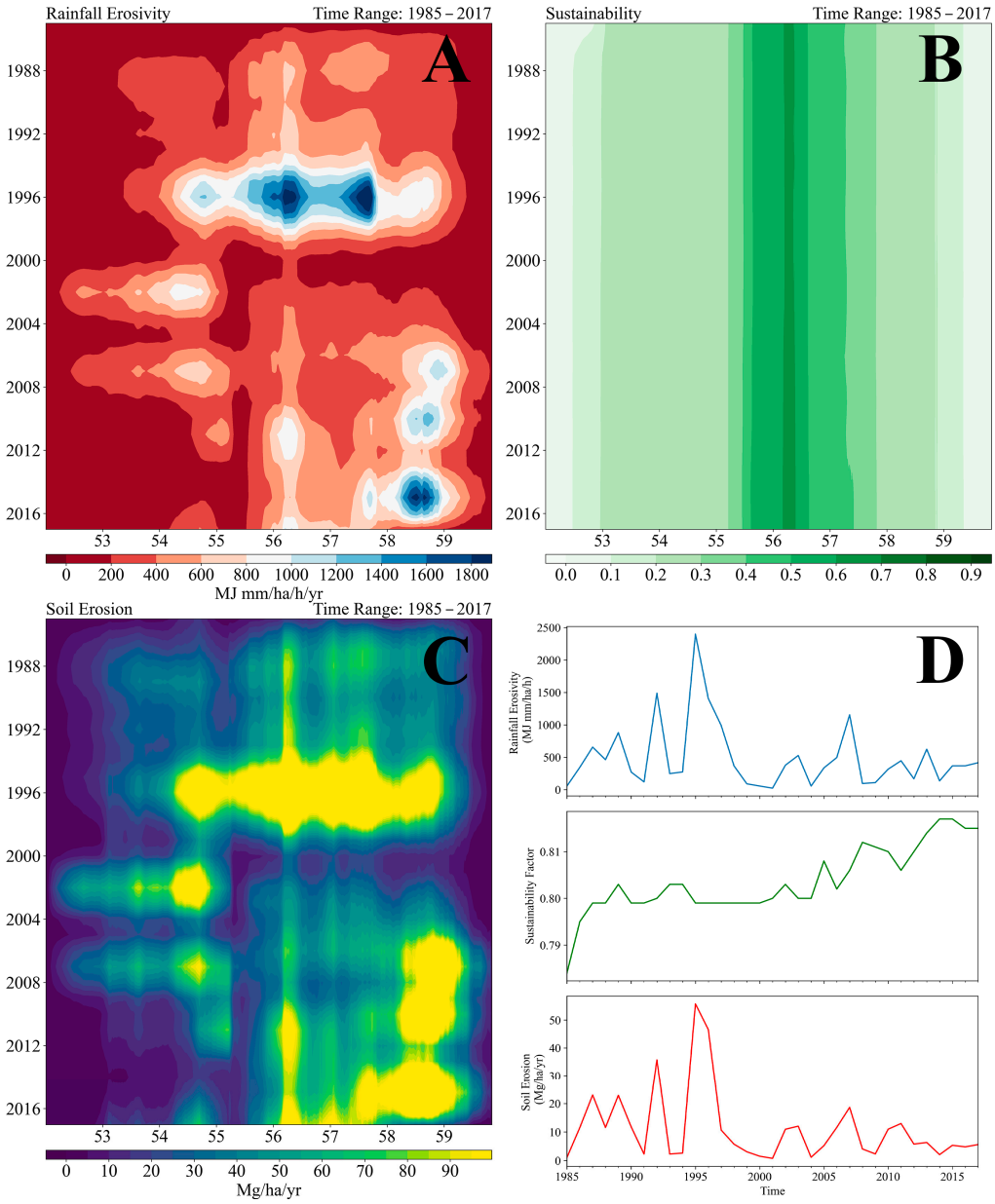

Figure 3. Hovmöller diagram of (**A**) rainfall erosivity (MJmmha^{-1}h^{-1}yr^{-1}), (**B**) sustainability (dimensionless), (**C**) soil erosion (Mgha^{-1}yr^{-1}), and (**D**) average time series between 1985 and 2017 in the Sultanate of Oman.

Rainfall erosivity is a challenging factor for estimation and is typically calculated based on daily, monthly, or annual precipitation using empirical equations. Higher time resolutions such as 1, 5, 15, 30, and 60 min analyses reveal lower rainfall erosivity values as time resolution increases [87]. However, the scarcity of precipitation data with proper time resolution (30 min or 60 min intervals) in Oman persuaded this study to use the model-based data of ERA5 Land Hourly, which is reanalysis data that combines observations with physical modeling of global atmospheric variables, including total precipitation between 1950 and 2021. Although recent advancements in satellite-based estimation provide rainfall data in 30 min intervals, the accuracy of satellite-based datasets such as CPC MORPHing technique (CMORPH) or Integrated Multi-satellitE Retrievals for GPM (IMERG) in capturing rainfall events in arid/semi-arid regions leads to the underestimation of rainfall erosivity [88–90]. Additionally, to compare our rainfall erosivity method with gauge-based estimation, we investigated the Global Rainfall Erosivity Database (GloREDa)

in Oman [91]. Therefore, we compared rainfall erosivity estimations based on ERA5, IMERG, and GloREDa between 2001 and 2010 (GloREDa temporal coverage), as shown in Figure 4. Results show that the rainfall erosivity estimation based on various methods has differences mostly in spatial distributions and range of values. These differences are rooted in the estimation procedure and the dataset accuracy. For example, GloREDa (Figure 4C) has several limitations, such as the lack of explicit observations in Oman and no consistent temporal coverage of WorldClim (as an interpolation covariate dataset between 1970 and 1990) and estimated rainfall erosivity in gauge observations (between 2000 and 2010), that limit GloREDa applicability and capability to accurately estimate rainfall erosivity. GloREDa is also based on an ML model configured by a Gaussian Process Regression (GPR) that used estimated rainfall erosivity on gauges in close proximity such as Iran and India to interpolate and extrapolate rainfall erosivity based on WorldClim variables that may lead to wrong estimations. As shown, the smooth rainfall erosivity estimations of GloREDa are completely different than IMERG and ERA5 (Figure 4A,B). On the other hand, the IMERG dataset is based on satellite observations that are just bias-corrected by gauge observations, and our analysis revealed that this dataset has poor capability to retrieve and detect rainfall over Oman (Table S1). However, ERA5 total precipitation has good agreement (Table 1) with gauge observations. Therefore, in this study, rainfall erosivity calculations were performed based on ERA5.

Table 1. Comparison between observation stations and ERA5 dataset.

Station	POD	CSI	MAE	RMSE	RBIAS	CC
Adam	0.81	0.56	0.05	0.79	5.68	0.75
Bahla	0.92	0.62	0.13	1.29	4.66	0.76
Diba	0.91	0.58	0.06	0.73	4.89	0.69
Fahud	0.82	0.49	0.02	0.32	2.37	0.90
Haima	0.86	0.47	0.01	0.19	−0.63	0.88
Ibra	0.91	0.64	0.12	1.11	6.64	0.85
Ibri	0.88	0.66	0.08	0.89	6.68	0.87
Jabal Shams	0.89	0.67	0.03	1.08	3.12	0.76
Joba	0.88	0.79	0.08	2.01	16.7	0.83
Khasab Port	0.92	0.68	0.11	0.45	5.77	0.79
Madha	0.82	0.58	0.16	1.21	6.27	0.91
Majis	0.93	0.56	0.09	0.78	0.83	0.89
Masirah	0.92	0.64	0.06	1.05	4.21	0.86
Nizwa	0.93	0.68	0.14	1.22	6.27	0.91
Qalhat	0.99	0.63	0.21	2.26	0.83	0.67
Rustaq	0.91	0.72	0.15	1.30	8.94	0.78
Saham	0.87	0.71	0.21	0.89	5.25	0.68
Saiq	0.91	0.65	0.18	1.63	5.28	0.82
Salalah	0.95	0.55	0.07	1.75	4.73	0.91
Samail	0.94	0.52	0.18	1.12	16.33	0.70
Sunaynah	0.96	0.63	0.08	0.80	5.31	0.87
Sur	0.97	0.68	0.13	1.44	9.05	0.69
Suwaiq	0.99	0.58	0.10	1.06	7.24	0.85
Thumrait	0.92	0.71	0.04	0.99	12.43	0.89
Yalooni	0.94	0.77	0.03	0.73	4.32	0.72
Yanqul	0.96	0.49	0.16	1.02	5.39	0.76
Average	0.91	0.62	0.10	1.08	6.09	0.81

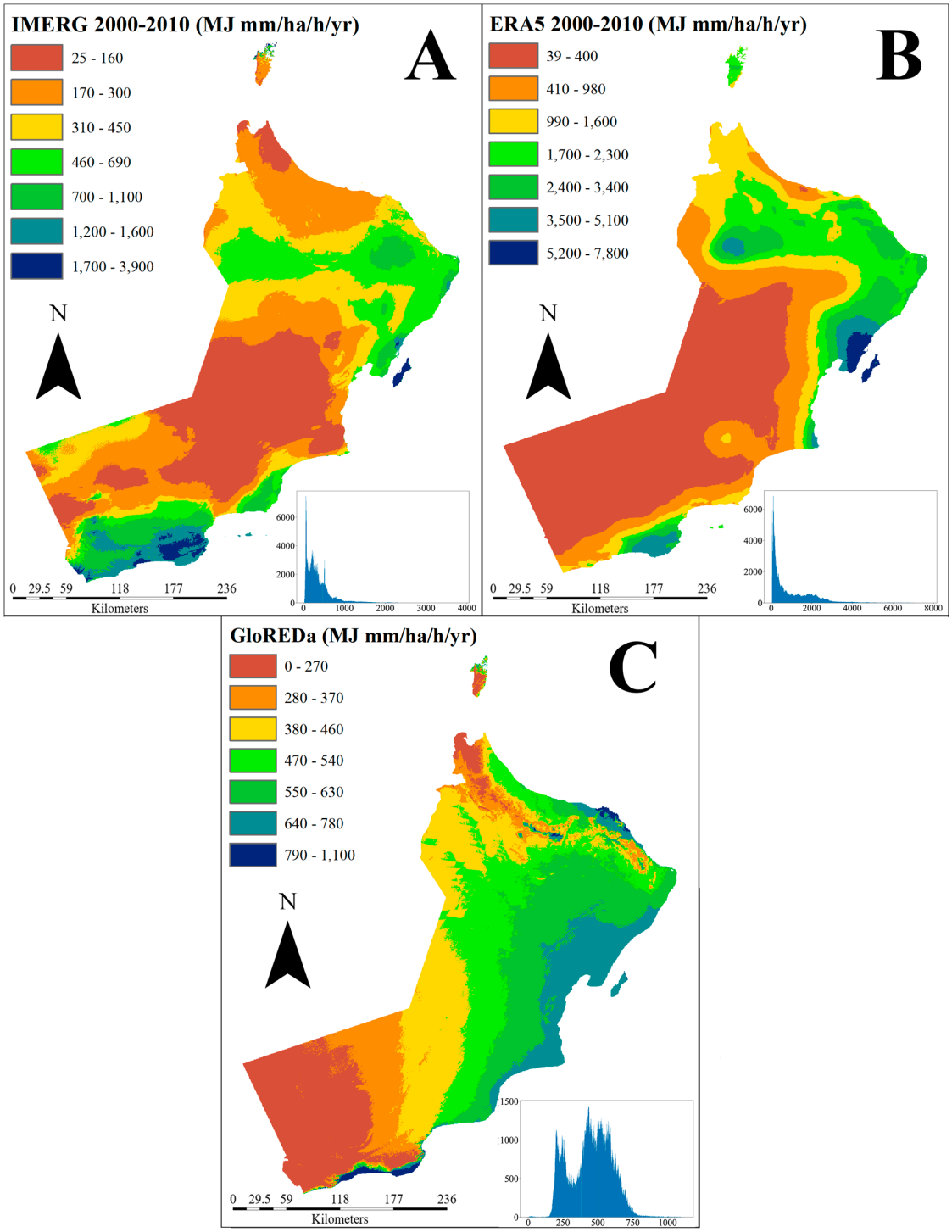

Figure 4. Rainfall erosivity of Oman between 2000 and 2010 by (**A**) IMERG dataset, (**B**) ERA5 dataset, and (**C**) GloREDa dataset. Note: rainfall erosivity based on gauge observations is interpolated by an ML model between 2000 and 2010 in GloREDa dataset, while rainfall erosivity for IMERG and ERA5 are shown to compare with GloREDa.

3.2. Sustainability Factor

We estimated the sustainability factor using a fraction of green vegetation cover and bare soil frequency using Sentinel 2 and composites of Landsat 5, 7, and 8 imageries to consider not only the vegetation effect but also the bareness of the lands to reflect the vegetation cover frequency through time and space (Figure 3B). Spatial variation of the

sustainability factor revealed that the desert lands of Oman typically have the highest values, while the mountain regions, which are covered by scattered vegetation in the north and dispersed shrubs and forests in the south, have the lowest values over time. Temporal variation indicates that the sustainability factor in some coastal regions increases as time progresses. It means forests, shrubs, or other sparse vegetation disappear over time, indicated by an increasing trend in the sustainability factor (Figure 3D). There is no explicit research to estimate sustainability or cover management factors in the study area, and land use–land cover datasets have ignored transitions of scattered vegetation in Oman. Therefore, as the G2 erosion model suggests this method's global applicability, we used this factor in the spatiotemporal estimation of soil erosion.

The sustainability factor is derived from the combination of cover management and practice management factors in the RUSLE equation. Various methods have been proposed to estimate cover management factors using either the NDVI-based formula or land use-land cover classes. However, these methods have been verified to agricultural extents. Hence, the major desert lands of Oman restricted the usage of these methods. Additionally, global or regional studies omitted the desert lands of the Sultanate of Oman in soil erosion estimations [28,92,93]. Therefore, the previous methods are not applicable in Oman.

3.3. Soil Erosion

Soil conservation programs generally consider acceptable soil erosion rates to be between 5 and 12 $Mgha^{-1}yr^{-1}$, or 0.4 to 1 $mmyr^{-1}$ of the soil surface layer [93]. Acceptable soil erosion rates are an index proposed by the United States Department of Agriculture (USDA) to maintain soil erosion while posing little risk to agricultural production. Because of political and economic considerations, several researchers expressed concern that these values represent higher-than-natural soil erosion production. However, in arid/semi-arid regions, the rate of soil formation is different. In arid/semi-arid regions that are mainly covered by barren lands and deserts, 10 cm of soil takes nearly 4000 years to form [93]; therefore, the highest tolerable soil erosion rate can be equal to the rate of soil formation from solid earth materials, equivalent to 2.2 $Mgha^{-1}yr^{-1}$ (0.17 $mmyr^{-1}$) [93]. However, average soil erosion values show that in 1996, with the highest rate of erosion (50 $Mgha^{-1}yr^{-1}$), the loss of topsoil surfaces reached 3.86 $mmyr^{-1}$, and for long-term average soil erosion (11 $Mgha^{-1}yr^{-1}$), the loss of topsoil surfaces was equal to 0.85 $mmyr^{-1}$. Notably, the loss of topsoil surfaces is an environmental hazard that puts soil health and stability in dangerous conditions (Figure 3C,D).

Spatiotemporal variation of soil erosion in Oman indicates that soil erosion closely follows the rainfall erosivity pattern over time and space (Figure 3C,D). The spatial variation shows the highest rates of soil erosion are in the northern and southern mountains and reach almost 700 ($Mgha^{-1}yr^{-1}$), which is extremely high. Desert lands, on the other hand, experience a lower rate of soil erosion (<10 $Mgha^{-1}yr^{-1}$) because, in most years, rainfall occurrence is the lowest. Rainfall erosivity shows that coastal areas are more susceptible to soil erosion, whereas the sustainability factor (considering land use) suggests that interior plateaus face a higher risk. The interaction between climate and land use variabilities is likely more complex. For example, although the highest soil erosion in mountain areas is mostly provoked by rainfall erosivity as the inducing erosion factor, the sparse vegetation coverage typically protects these areas (Figure 5A,B). Therefore, there should be another parameter that may rule in these areas. G2 erosion factors such as soil erodibility and terrain influence in mountain areas play crucial roles (Figure 5C,D). These erosion factors have changed soil erosion patterns in some regions such as the mountains. With low values of soil erodibility (0.024 $MghahMJ^{-1}ha^{-1}mm^{-1}$) and high values of terrain factor (>10) combined with maximum rainfall erosivity values, the highest rate of soil erosion through time and space occurs in these regions, though they are covered by sparse forests. The interior plateaus show similar patterns, with low soil erosion values where terrain influence is extremely low due to flat regions of barren lands. However, the sustainability factor indicates the highest susceptibility to erosion is in these areas.

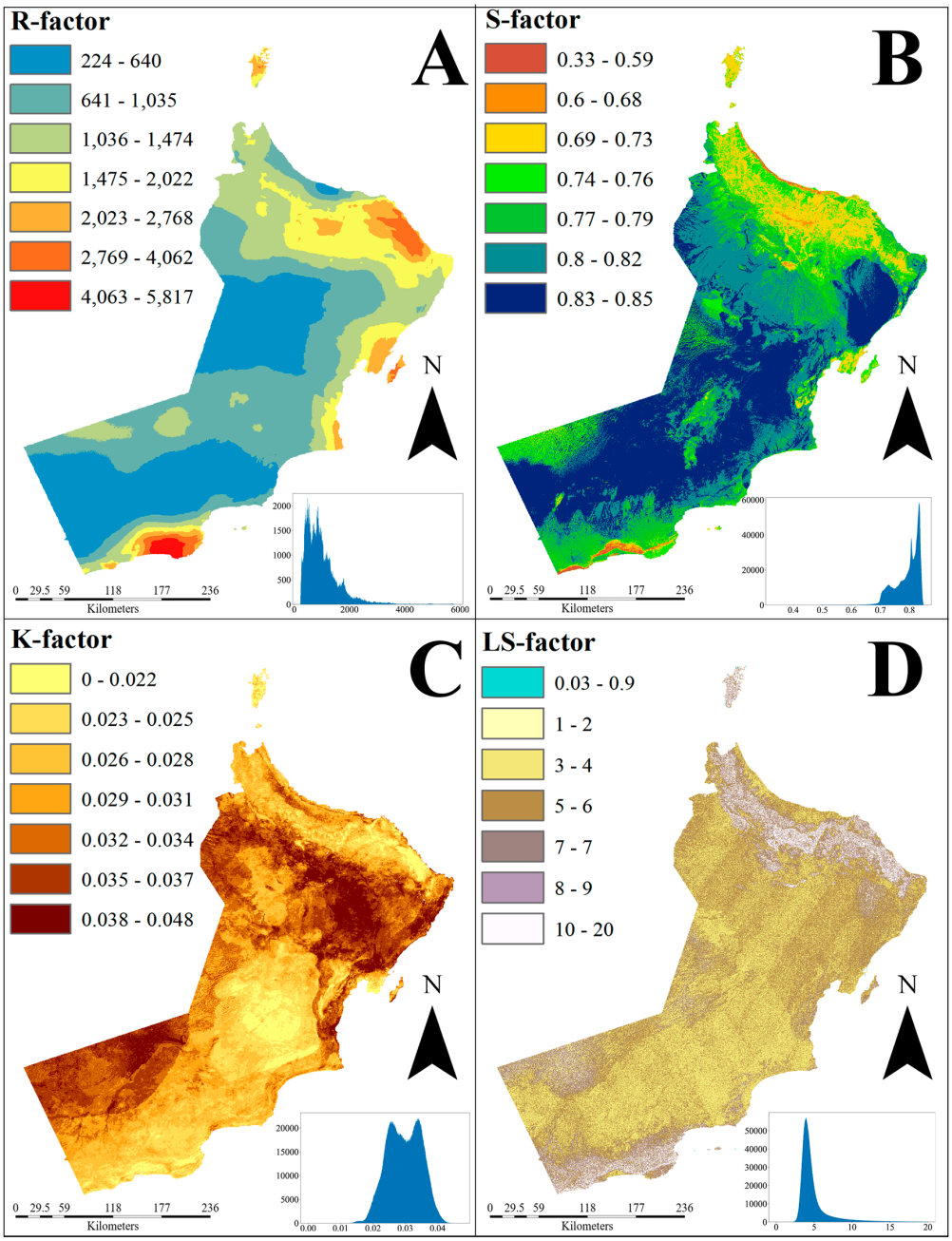

Figure 5. G2 erosion model factors. (**A**) rainfall erosivity (MJmmha^{-1}h^{-1}yr^{-1}), (**B**) average sustainability factor, (**C**) soil erodibility (MghahMJ^{-1}ha^{-1}mm^{-1}), (**D**) terrain influence.

Soil erosion estimation in arid/semi-arid regions is challenging, and the major problem is estimating soil erosion factors. For example, estimations of rainfall erosivity and sustainability factors face various problems in validation because most of the lands are barren, and previous studies have ignored these lands in soil erosion estimations [28,92,94,95]. Therefore, there is no study of soil erosion in the desert lands of Oman to verify the results quantitatively. However, some studies such as Global Assessment of Soil Degradation (GLASOD) and Global Forest Watch Erosion (GFWE) have generated erosion risk maps to qualitatively verify our study [96,97] (Figure 6). The comparisons show that this study represents a similar spatial distribution of soil erosion, except GLASOD does not represent soil erosion in the desert and active dune lands, while GFWE proposed these lands had the lowest risks of erosion, which is similar to our study. These studies also display that the highest risk of soil erosion is on the tops of mountains, where terrain influence is

greatest, and that the risk is lowest in barren lands, due to lower rainfall erosivity and terrain influence. Some differences may exist because GLASOD examined soil erosion between 1977 and 1980, GFWE investigated soil erosion risk between 2001 and 2011, and our study evaluated temporal coverage between 1985 and 2017. The GLASOD and GFWE showed the hotspots of soil erosion should be at the highest altitudes, and our study has good agreement with these studies. However, our study suggests soil erosion in coastal regions is also high, mostly in terms of monsoon rainfalls characterized by the rainfall erosivity factor.

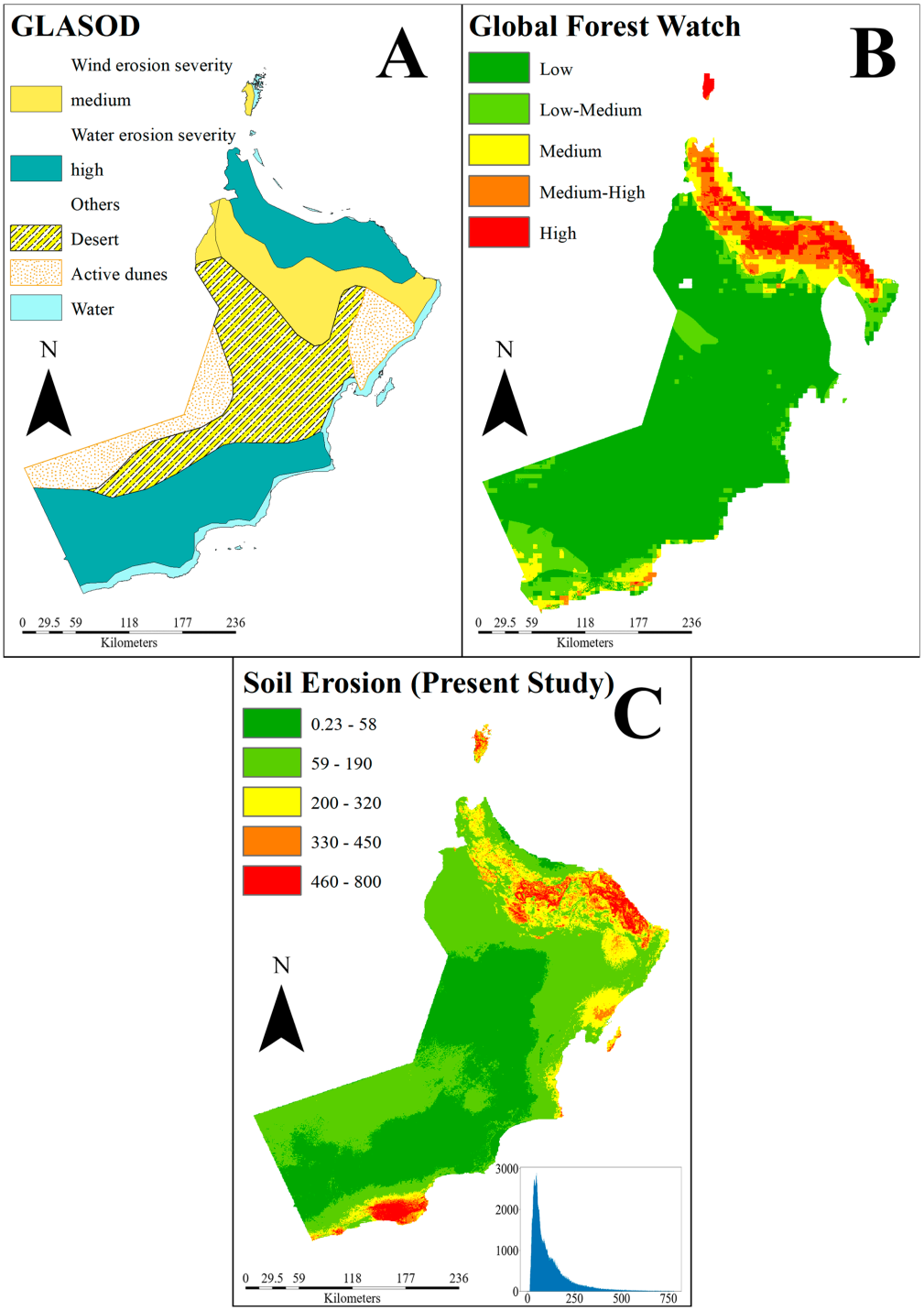

Figure 6. Average soil erosion map of Oman. (**A**) GLASOD dataset, (**B**) GFWE dataset, (**C**) present study.

3.4. Soil Erosion Hazard Maps

According to the United Nations Convention to Combat Desertification (UNCCD) [10], soil erosion is a major contributor to desertification in arid/semi-arid regions such as Oman. Therefore, soil erosion hazards in these marginal environments should be investigated for socio-economic and sustainable development. At the same time, climate change and urban area expansion may lead to social and environmental problems. To help policymakers with sustainable strategies for land management purposes and soil erosion hazards within the specific time of occurrence, we used the EVA method to investigate soil erosion hazards for various return periods (Figure 7). For instance, regarding the soil erosion hazards in the 5-year return period, the maximum soil erosion value reaches 600 ($Mgha^{-1}yr^{-1}$), which is lower than the average values between 1985 and 2017 (Figure 7A), while the soil erosion hazard in the 10-year return period (1400 $Mgha^{-1}yr^{-1}$) will exceed average values (Figure 7B). The extreme values in the 25- and 50-year return periods will reach maximum values of 3000 and 8000 ($Mgha^{-1}yr^{-1}$) return intervals, which are extremely high and warn land managers about extreme events that may happen in the worst conditions (Figure 7C,D). These high values of soil erosion are primarily associated with ripples and sand dunes in dry regions. This indicates that, although the average soil erosion in these areas is not particularly high, the LS-factor becomes significantly influential during higher return periods, dramatically increasing soil erosion values for the 25- and 50-year return periods. Additionally, climate change and land use alterations have altered soil erosion patterns in the Sultanate of Oman between 1985 and 2017. For instance, the southwestern regions (e.g., Dhofar) have experienced an increasing intensity of soil erosion, primarily due to heightened rainfall intensity (extreme monsoons) and deforestation. Therefore, while soil erodibility and terrain influence govern interior plateaus, the variations in rainfall erosivity and sustainability factors are the dynamic factors that alter the soil erosion patterns and trends and modify soil erosion hazards. For example, as return intervals increase, areas with lower susceptibility to erosion, such as the interior plateau of desert lands (that reach a maximum of 500 $Mgha^{-1}yr^{-1}$) increase with gentle slopes, while the areas with higher susceptibility to erosion, such as mountain areas or sand dunes, increase with steep slopes, which is mainly due to changes in climate and land use alterations. Therefore, the hazardous maps of soil erosion could help policymakers focus on mountains, sand dunes, and eastern shorelines to design and manage lands against soil erosion and degradation. The histogram of soil erosion for each return period also shows increasing hazardous return levels; however, the frequency of the lowest values all over Oman does not change significantly. Although the distribution of soil erosion frequency has not changed between 5 and 10 years of the return period, by increasing return periods to 25 and 50 years, the soil erosion distribution changes, and two intervals of erosion are more probable, as well as soil erosion hazards. These differences in extreme intervals of soil erosion show some areas that were susceptible to erosion in 5 or 10 years of return periods. These areas, such as the northern coastal line, will have lower susceptibility to erosion, while other areas, such as the sand dunes in the north of the southern regions, are more susceptible to erosion.

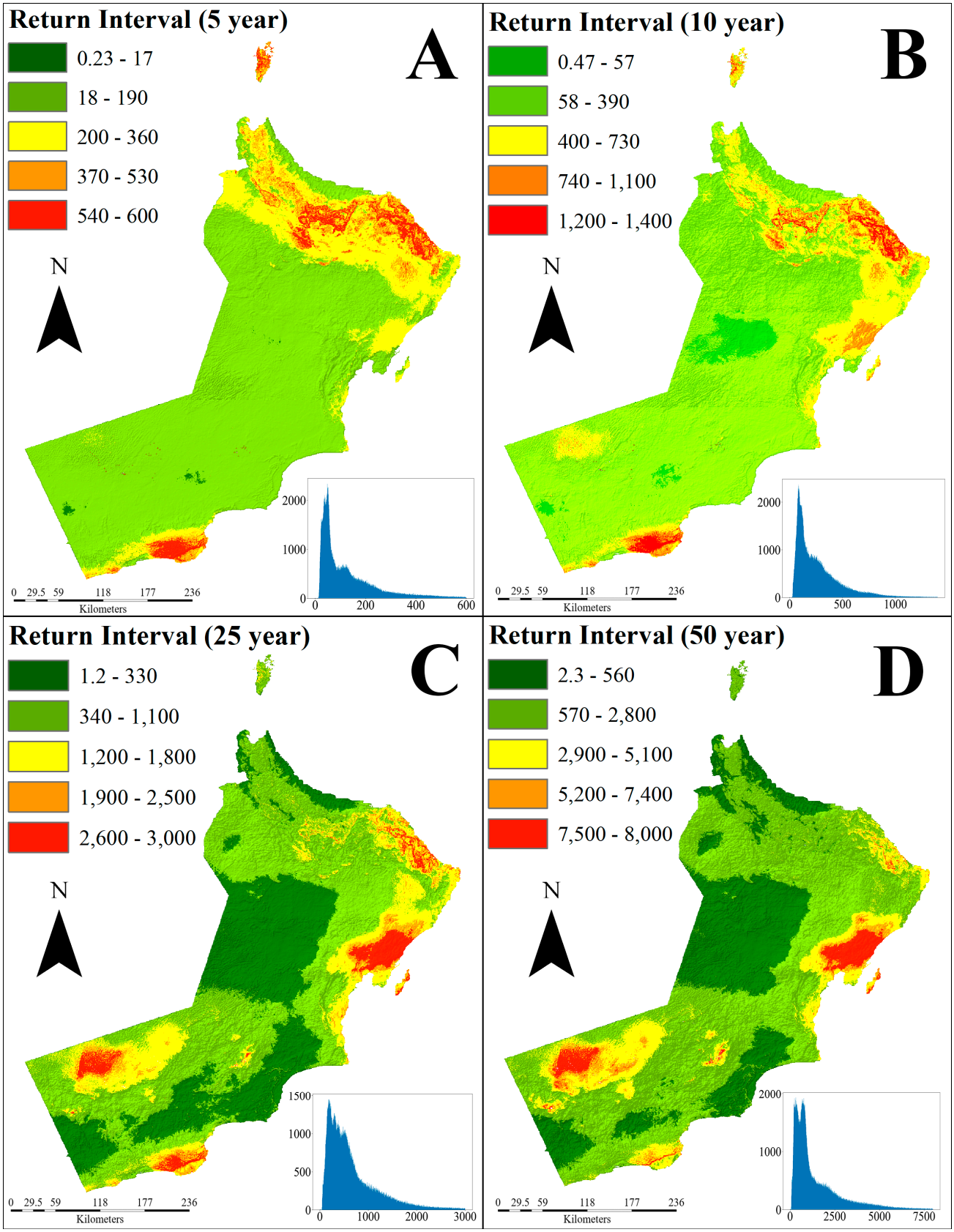

Figure 7. Soil erosion hazard map ($Mgha^{-1}yr^{-1}$) of Oman for return periods of (**A**) 5 years, (**B**) 10 years, (**C**) 25 years, and (**D**) 50 years.

4. Conclusions

We used the G2 (modified RUSLE) erosion model to estimate the spatiotemporal variation of soil erosion in the Sultanate of Oman. Rainfall erosivity was estimated based on an RF model and ERA5 Land Hourly dataset between 1985 and 2017. We used Sentinel 2 and Landsat 5, 7, and 8 composite imageries to estimate sustainability variation in the Sultanate of Oman. Soil erosion hazard maps were generated for each region for various return periods using EVA analysis that considers the frequency and patterns of historical events.

Although the proposed method inherits the G2 erosion model and ERA5 dataset's uncertainty and limitations, it has some advantages and disadvantages as follows:

1. The proposed method can be used globally to estimate and assess soil erosion risks.
2. The proposed method can investigate soil erosion hazards based on the likelihood of historical trends and frequency using the EVA method.
3. This study can assist policymakers in justifying soil erosion in environmental regions that lack regional datasets worldwide.
4. The proposed method estimates sustainability factors using Sentinel 2 and composites of Landsat 5, 7, and 8 that make it possible to be estimated on a global scale.
5. Results identified that climate variability is the primary driver of dynamics in soil erosion and associated hazards. However, soil erosion can also be influenced by changes in land use and land cover (LULC).
6. The static factors of soil erodibility and terrain can adversely impact soil erosion hazards, although they remain closely influenced by climate variations and land use/land cover (LULC) changes. Consequently, these factors hold secondary priority in areas prone to soil erosion hazards.

Supplementary Materials: The following supporting information can be downloaded at: https://www.mdpi.com/article/10.3390/rs16162976/s1.

Author Contributions: Conceptualization: S.A.S. and M.A.-W., Methodology: S.A.S., M.G.M. and M.R.N., Supervision: M.A.-W. and M.R.N., Writing—Review and Editing: S.A.S., M.A.-W., M.R.N., N.A., N.T. and A.H.G. All authors have read and agreed to the published version of the manuscript.

Funding: This study is funded by the Ministry of Environment and Climate Affairs (Environment Authority) of the Sultanate of Oman, under the Project for Mapping, Monitoring, and Mitigation of Land Degradation in Oman (CR/AGR/SWAE/13/02), awarded to Sultan Qaboos University, Oman.

Data Availability Statement: The raw data supporting the conclusions of this article will be made available by the authors on request.

Conflicts of Interest: The authors declare no conflicts of interest.

References

1. Pimentel, D. *World Soil Erosion and Conservation*; Cambridge University Press: Cambridge, UK, 1993.
2. Eswaran, H.; Reich, P.F. Land Degradation: An Overview. NRCS Soils. Available online: http://soils.usda.gov/use/worldsoils/papers/land-degradation-overview.html (accessed on 22 January 2021).
3. Aslam, B.; Maqsoom, A.; Shahzaib; Kazmi, Z.A.; Sodangi, M.; Anwar, F.; Bakri, M.H.; Tufail, R.F.; Farooq, D. Effects of Landscape Changes on Soil Erosion in the Built Environment: Application of Geospatial-Based RUSLE Technique. *Sustainability* **2020**, *12*, 5898. [CrossRef]
4. Bowker, M.A.; Belnap, J.; Bala Chaudhary, V.; Johnson, N.C. Revisiting Classic Water Erosion Models in Drylands: The Strong Impact of Biological Soil Crusts. *Soil Biol. Biochem.* **2008**, *40*, 2309–2316. [CrossRef]
5. Yang, D.; Kanae, S.; Oki, T.; Koike, T.; Musiake, K. Global potential soil erosion with reference to land use and climate changes. *Hydrol. Process.* **2003**, *17*, 2913–2928. [CrossRef]
6. Rostagno, C.M.; Degorgue, G. Desert Pavements as Indicators of Soil Erosion on Aridic Soils in North-East Patagonia (Argentina). *Geomorphology* **2011**, *134*, 224–231. [CrossRef]
7. Marondedze, A.K.; Schütt, B. Assessment of Soil Erosion Using the Rusle Model for the Epworth District of the Harare Metropolitan Province, Zimbabwe. *Sustainability* **2020**, *12*, 8531. [CrossRef]
8. Oliver, M.A.; Gregory, P.J. Soil, Food Security and Human Health: A Review. *Eur. J. Soil Sci.* **2014**, *66*, 257–276. [CrossRef]
9. Zhang, Y.-G.; Nearing, M.A.; Zhang, X.-C.; Xie, Y.; Wei, H. Projected Rainfall Erosivity Changes under Climate Change from Multimodel and Multiscenario Projections in Northeast China. *J. Hydrol.* **2010**, *384*, 97–106. [CrossRef]

10. Ma, H.; Zhao, H. United Nations: Convention to Combat Desertification in Those Countries Experiencing Serious Drought and/or Desertification, Particularly in Africa. *Int. Legal Mater.* **1994**, *33*, 1328–1382.
11. Gourfi, A.; Daoudi, L. Effects of Land Use Changes on Soil Erosion and Sedimentation of Dams in Semi-Arid Regions: Example of N'Fis Watershed in Western High Atlas. *J. Earth Sci. Clim. Chang.* **2019**, *10*, 513. [CrossRef]
12. Peng, J.-F.; Song, Y.-H.; Yuan, P.; Cui, X.-Y.; Qiu, G.-L. The Remediation of Heavy Metals Contaminated Sediment. *J. Hazard. Mater.* **2009**, *161*, 633–640. [CrossRef]
13. Wu, G.-L.; Liu, Y.-F.; Cui, Z.; Liu, Y.; Shi, Z.-H.; Yin, R.; Kardol, P. Trade-off between Vegetation Type, Soil Erosion Control and Surface Water in Global Semi-Arid Regions: A Meta-Analysis. *J. Appl. Ecol.* **2020**, *57*, 875–885. [CrossRef]
14. Ziadat, F.M.; Taimeh, A.Y. Effect of Rainfall Intensity, Slope, Land Use and Antecedent Soil Moisture on Soil Erosion in an Arid Environment. *Land Degrad. Dev.* **2013**, *24*, 582–590. [CrossRef]
15. Simonneaux, V.; Cheggour, A.; Deschamps, C.; Mouillot, F.; Cerdan, O.; Le Bissonnais, Y. Land Use and Climate Change Effects on Soil Erosion in a Semi-Arid Mountainous Watershed (High Atlas, Morocco). *J. Arid Environ.* **2015**, *122*, 64–75. [CrossRef]
16. Kairis, O.; Karavitis, C.; Salvati, L.; Kounalaki, A.; Kosmas, K. Exploring the Impact of Overgrazing on Soil Erosion and Land Degradation in a Dry Mediterranean Agro-Forest Landscape (Crete, Greece). *Arid Land Res. Manag.* **2015**, *29*, 360–374. [CrossRef]
17. Wen, X. Temporal and Spatial Relationships between Soil Erosion and Ecological Restoration in Semi-Arid Regions: A Case Study in Northern Shaanxi, China. *GIScience Remote Sens.* **2020**, *57*, 572–590. [CrossRef]
18. Ganasri, B.P.; Ramesh, H. Assessment of Soil Erosion by RUSLE Model Using Remote Sensing and GIS—A Case Study of Nethravathi Basin. *Geosci. Front.* **2016**, *7*, 953–961. [CrossRef]
19. Han, X.; Xiao, J.; Wang, L.; Tian, S.; Liang, T.; Liu, Y. Identification of Areas Vulnerable to Soil Erosion and Risk Assessment of Phosphorus Transport in a Typical Watershed in the Loess Plateau. *Sci. Total Environ.* **2020**, *758*, 143661. [CrossRef]
20. Berberoglu, S.; Cilek, A.; Kirkby, M.; Irvine, B.; Donmez, C. Spatial and Temporal Evaluation of Soil Erosion in Turkey under Climate Change Scenarios Using the Pan-European Soil Erosion Risk Assessment (PESERA) Model. *Environ. Monit. Assess.* **2020**, *192*, 491. [CrossRef] [PubMed]
21. der Knijff, J.M.; Jones, R.J.A.; Montanarella, L. *Soil Erosion Risk: Assessment in Europe*; European Soil Bureau: Ispra, Italy, 2000.
22. Teng, H.; Liang, Z.; Chen, S.; Liu, Y.; Viscarra Rossel, R.A.; Chappell, A.; Yu, W.; Shi, Z. Current and Future Assessments of Soil Erosion by Water on the Tibetan Plateau Based on RUSLE and CMIP5 Climate Models. *Sci. Total Environ.* **2018**, *635*, 673–686. [CrossRef]
23. Borrelli, P.; Robinson, D.A.; Panagos, P.; Lugato, E.; Yang, J.E.; Alewell, C.; Wuepper, D.; Montanarella, L.; Ballabio, C. Land Use and Climate Change Impacts on Global Soil Erosion by Water (2015–2070). *Proc. Natl. Acad. Sci. USA* **2020**, *117*, 21994–22001. [CrossRef]
24. Karydas, C.G.; Panagos, P. The G2 Erosion Model: An Algorithm for Month-Time Step Assessments. *Environ. Res.* **2018**, *161*, 256–267. [CrossRef] [PubMed]
25. Segura, C.; Sun, G.; McNulty, S.; Zhang, Y. Potential Impacts of Climate Change on Soil Erosion Vulnerability across the Conterminous United States. *J. Soil Water Conserv.* **2014**, *69*, 171–181. [CrossRef]
26. Jin, F.; Yang, W.; Fu, J.; Li, Z. Effects of Vegetation and Climate on the Changes of Soil Erosion in the Loess Plateau of China. *Sci. Total Environ.* **2021**, *773*, 145514. [CrossRef] [PubMed]
27. Borrelli, P.; Robinson, D.A.; Fleischer, L.R.; Lugato, E.; Ballabio, C.; Alewell, C.; Meusburger, K.; Modugno, S.; Schütt, B.; Ferro, V.; et al. An Assessment of the Global Impact of 21st Century Land Use Change on Soil Erosion. *Nat. Commun.* **2017**, *8*, 2013. [CrossRef] [PubMed]
28. Xiong, M.; Sun, R.; Chen, L. A global comparison of soil erosion associated with land use and climate type. *Geoderma* **2019**, *343*, 31–39. [CrossRef]
29. Atoma, H.; Suryabhagavan, K.V.; Balakrishnan, M. Soil Erosion Assessment Using RUSLE Model and GIS in Huluka Watershed, Central Ethiopia. *Sustain. Water Resour. Manag.* **2020**, *6*, 12. [CrossRef]
30. Bartley, R.; Corfield, J.P.; Abbott, B.N.; Hawdon, A.A.; Wilkinson, S.N.; Nelson, B. Impacts of Improved Grazing Land Management on Sediment Yields, Part 1: Hillslope Processes. *J. Hydrol.* **2010**, *389*, 237–248. [CrossRef]
31. Woznicki, S.A.; Cada, P.; Wickham, J.; Schmidt, M.; Baynes, J.; Mehaffey, M.; Neale, A. Sediment Retention by Natural Landscapes in the Conterminous United States. *Sci. Total Environ.* **2020**, *745*, 140972. [CrossRef] [PubMed]
32. Phippen, S.J.; Wohl, E. An Assessment of Land Use and Other Factors Affecting Sediment Loads in the Rio Puerco Watershed, New Mexico. *Geomorphology* **2003**, *52*, 269–287. [CrossRef]
33. Brady, N.C.; Weil, R.R. *The Nature and Properties of Soils*, 14th ed.; Prentice-Hall: Upper Saddle River, NJ, USA, 2008; ISBN 9780132279390.
34. Renard, K.G.; Foster, G.R.; Weesies, G.A.; Porter, J.P. RUSLE: Revised Universal Soil Loss Equation. *J. Soil Water Conserv.* **1991**, *46*, 30–33. [CrossRef]
35. de la Rosa, D.; Moreno, J.A.; Mayol, F.; Bonsón, T. Assessment of Soil Erosion Vulnerability in Western Europe and Potential Impact on Crop Productivity Due to Loss of Soil Depth Using the ImpelERO Model. *Agric. Ecosyst. Environ.* **2000**, *81*, 179–190. [CrossRef]
36. Nicks, A.D.; Lane, L.J.; Gander, G.A. Weather Generator. In *Water Erosion Prediction Project: Hillslope Profile and Watershed Model Documentation*; United States Department of Agriculture: West Lafayette, IN, USA, 1995.

37. Rahman, M.R.; Shi, Z.H.; Chongfa, C.; Dun, Z. Assessing Soil Erosion Hazard -a Raster Based GIS Approach with Spatial Principal Component Analysis (SPCA). *Earth Sci. Inform.* **2015**, *8*, 853–865. [CrossRef]
38. Zhang, Y.; Schaap, M.G.; Zha, Y. A High-Resolution Global Map of Soil Hydraulic Properties Produced by a Hierarchical Parameterization of a Physically Based Water Retention Model. *Water Resour. Res.* **2018**, *54*, 9774–9790. [CrossRef]
39. Huang, W.; Ho, H.C.; Peng, Y.; Li, L. Qualitative Risk Assessment of Soil Erosion for Karst Landforms in Chahe Town, Southwest China: A Hazard Index Approach. *Catena* **2016**, *144*, 184–193. [CrossRef]
40. Chen, S.; Liu, W.; Bai, Y.; Luo, X.; Li, H.; Zha, X. Evaluation of Watershed Soil Erosion Hazard Using Combination Weight and GIS: A Case Study from Eroded Soil in Southern China. *Nat. Hazard.* **2021**, *109*, 1603–1628. [CrossRef]
41. Bewket, W.; Teferi, E. Assessment of Soil Erosion Hazard and Prioritization for Treatment at the Watershed Level: Case Study in the Chemoga Watershed, Blue Nile Basin, Ethiopia. *Land Degrad. Dev.* **2009**, *20*, 609–622. [CrossRef]
42. Lu, H.; Moran, C.J.; Prosser, I.P.; Raupach, M.R.; Olley, J.; Petheram, C. Hillslope Erosion and Sediment Delivery: A Basin Wide Estimation at Medium Catchment Scale. 2003. Available online: https://scholar.google.com/scholar?hl=en&as_sdt=0,5&q=Hillslope+Erosion+and+Sediment+Delivery:+A+Basin+Wide+Estimation+at+Medium+Catchment+Scale+&btnG= (accessed on 6 August 2024).
43. Rahman, M.R.; Shi, Z.H.; Chongfa, C. Soil Erosion Hazard Evaluation-An Integrated Use of Remote Sensing, GIS and Statistical Approaches with Biophysical Parameters towards Management Strategies. *Ecol. Model.* **2009**, *220*, 1724–1734. [CrossRef]
44. Senanayake, S.; Pradhan, B.; Huete, A.; Brennan, J. A Review on Assessing and Mapping Soil Erosion Hazard Using Geo-Informatics Technology for Farming System Management. *Remote Sens.* **2020**, *12*, 4063. [CrossRef]
45. Almagro, A.; Oliveira, P.T.S.; Nearing, M.A.; Hagemann, S. Projected Climate Change Impacts in Rainfall Erosivity over Brazil. *Sci. Rep.* **2017**, *7*, 8130. [CrossRef]
46. Hoomehr, S.; Schwartz, J.S.; Yoder, D.C. Potential Changes in Rainfall Erosivity under GCM Climate Change Scenarios for the Southern Appalachian Region, USA. *Catena* **2016**, *136*, 141–151. [CrossRef]
47. Zhang, X.C.; Nearing, M.A. Impact of Climate Change on Soil Erosion, Runoff, and Wheat Productivity in Central Oklahoma. *Catena* **2005**, *61*, 185–195. [CrossRef]
48. Panagos, P.; Karydas, C.; Borrelli, P.; Ballabio, C.; Meusburger, K. Advances in Soil Erosion Modelling through Remote Sensing Data Availability at European Scale. In Proceedings of the Second International Conference on Remote Sensing and Geoinformation of the Environment (RSCy2014), Paphos, Cyprus, 7–10 April 2014; Hadjimitsis, D.G., Themistocleous, K., Michaelides, S., Papadavid, G., Eds.; SPIE: Bellingham, WA, USA, 2014; Volume 9229, pp. 119–128.
49. Meliho, M.; Khattabi, A.; Mhammdi, N. Spatial Assessment of Soil Erosion Risk by Integrating Remote Sensing and GIS Techniques: A Case of Tensift Watershed in Morocco. *Environ. Earth Sci.* **2020**, *79*, 207. [CrossRef]
50. Pandey, A.; Mathur, A.; Mishra, S.K.; Mal, B.C. Soil Erosion Modeling of a Himalayan Watershed Using RS and GIS. *Environ. Earth Sci.* **2009**, *59*, 399–410. [CrossRef]
51. Prasannakumar, V.; Vijith, H.; Abinod, S.; Geetha, N. Estimation of Soil Erosion Risk within a Small Mountainous Sub-Watershed in Kerala, India, Using Revised Universal Soil Loss Equation (RUSLE) and Geo-Information Technology. *Geosci. Front.* **2012**, *3*, 209–215. [CrossRef]
52. Yang, X.; Zhang, X.; Lv, D.; Yin, S.; Zhang, M.; Zhu, Q.; Yu, Q.; Liu, B. Remote Sensing Estimation of the Soil Erosion Cover-Management Factor for China's Loess Plateau. *Land Degrad. Dev.* **2020**, *31*, 1942–1955. [CrossRef]
53. Cama, M.; Schillaci, C.; Kropáček, J.; Hochschild, V.; Bosino, A.; Märker, M. A Probabilistic Assessment of Soil Erosion Susceptibility in a Head Catchment of the Jemma Basin, Ethiopian Highlands. *Geosciences* **2020**, *10*, 248. [CrossRef]
54. Panagos, P.; Ballabio, C.; Poesen, J.; Lugato, E.; Scarpa, S.; Montanarella, L.; Borrelli, P. A Soil Erosion Indicator for Supporting Agricultural, Environmental and Climate Policies in the European Union. *Remote Sens.* **2020**, *12*, 1365. [CrossRef]
55. Kim, J.; Han, H.; Kim, B.; Chen, H.; Lee, J.H. Use of a High-Resolution-Satellite-Based Precipitation Product in Mapping Continental-Scale Rainfall Erosivity: A Case Study of the United States. *Catena* **2020**, *193*, 104602. [CrossRef]
56. Leh, M.; Bajwa, S.; Chaubey, I. Impact of Land Use Change on Erosion Risk: An Integrated Remote Sensing, Geographic Information System and Modeling Methodology. *Land Degrad. Dev.* **2011**, *24*, 409–421. [CrossRef]
57. Karaburun, A. Estimation of C Factor for Soil Erosion Modeling Using NDVI in Buyukcekmece Watershed. *Ozean J. Appl. Sci.* **2010**, *3*, 77–85.
58. Sepuru, T.K.; Dube, T. An Appraisal on the Progress of Remote Sensing Applications in Soil Erosion Mapping and Monitoring. *Remote Sens. Appl. Soc. Environ.* **2018**, *9*, 1–9. [CrossRef]
59. Wischmeier, W.H.; Smith, D.D. *Predicting Rainfall-Erosion Losses from Cropland East of the Rocky Mountains*; United States Department of Agriculture—Agricultural Research Service: Washington, DC, USA, 1979; Volume 282.
60. Fernandez, C.; Wu, J.Q.; McCool, D.K.; Stöckle, C.O. Estimating Water Erosion and Sediment Yield with GIS, RUSLE, and SEDD. *J. Sci. Water Conserv.* **2003**, *58*, 128–136.
61. Roy, D.P.; Kovalskyy, V.; Zhang, H.K.; Vermote, E.F.; Yan, L.; Kumar, S.S.; Egorov, A. Characterization of Landsat-7 to Landsat-8 Reflective Wavelength and Normalized Difference Vegetation Index Continuity. *Remote Sens. Environ.* **2016**, *185*, 57–70. [CrossRef] [PubMed]
62. Chuenchum, P.; Xu, M.; Tang, W. Estimation of Soil Erosion and Sediment Yield in the Lancang-Mekong River Using the Modified Revised Universal Soil Loss Equation and GIS Techniques. *Water* **2020**, *12*, 135. [CrossRef]

63. Desmet, P.J.J.; Govers, G. A GIS Procedure for Automatically Calculating the USLE LS Factor on Topographically Complex Landscape Units. *J. Soil Water Conserv.* **1996**, *51*, 427–433.
64. Foster, G.R.; Wischmeier, W.H. Evaluating Irregular Slopes for Soil Loss Prediction. *Trans. ASAE* **1974**, *17*, 305–309. [CrossRef]
65. Wischmeier, W.H.; Smith, D.D. *Predicting Rainfall Erosion Losses: A Guide to Conservation Planning (No. 537)*; Department of Agriculture, Science and Education: Port Antonio, Jamaica, 1978.
66. Brown, L.C.; Foster, G.R. Storm Erosivity Using Idealized Intensity Distributions. *Trans. ASAE* **1987**, *30*, 379. [CrossRef]
67. Nearing, M.A.; Yin, S.Q.; Borrelli, P.; Polyakov, V.O. Rainfall Erosivity: An Historical Review. *Catena* **2017**, *157*, 357–362. [CrossRef]
68. Rosewell, C.J. Rainfall Kinetic Energy in Eastern Australia. *J. Appl. Meteorol. Climatol.* **1986**, *25*, 1695–1701. [CrossRef]
69. Foster, G.R.; Yoder, D.C.; Weesies, G.A.; McCool, D.K.; McGregor, K.C.; Bingner, R.L. *RUSLE2 User's Guide*; United States Department of Agriculture—Agricultural Research Service: Washington, DC, USA, 2003.
70. Dabley, S.; Justice, V. *RIST-Rainfall Intensity Summarization Tool, Version 3.6*; United States Department of Agriculture—Agricultural Research Service: Washington, DC, USA, 2012.
71. Muñoz-Sabater, J.; Dutra, E.; Agustí-Panareda, A.; Albergel, C.; Arduini, G.; Balsamo, G.; Boussetta, S.; Choulga, M.; Harrigan, S.; Hersbach, H.; et al. ERA5-Land: A State-of-the-Art Global Reanalysis Dataset for Land Applications. *Earth Syst. Sci. Data* **2021**, *13*, 4349–4383. [CrossRef]
72. Karger, D.N.; Conrad, O.; Böhner, J.; Kawohl, T.; Kreft, H.; Soria-Auza, R.W.; Zimmermann, N.E.; Linder, H.P.; Kessler, M. Climatologies at High Resolution for the Earth's Land Surface Areas. *Sci. Data* **2017**, *4*, 170122. [CrossRef] [PubMed]
73. Breiman, L.; Friedman, J.; Olshen, R.A.; Stone, C.J. *Classification and Regression Trees*; Chapma and Hall: New York, NY, USA, 1984.
74. Bergsma, E. Aspects of Mapping Units in the Rain Erosion Hazard Catchment Survey. In *Land Evaluation for Land Use Planning and Conservation in Sloping Areas*; International Institute for Land Reclamation and Improvement: Wageningen, The Netherlands, 1986; pp. 84–105.
75. Simons, G.; Koster, R.; Droogers, P. *HiHydroSoil v2. 0-High Resolution Soil Maps of Global Hydraulic Properties*; FutureWater: Wageningen, The Netherlands, 2020.
76. Poggio, L.; de Sousa, L.M.; Batjes, N.H.; Heuvelink, G.B.M.; Kempen, B.; Riberio, E.; Rossiter, D. SoilGrids 2.0: Producing Quality-Assessed Soil Information for the Globe. *Soil* **2020**, *7*, 217–240. [CrossRef]
77. Jones, R.J.A.; Spoor, G.; Thomasson, A.J. Vulnerability of Subsoils in Europe to Compaction: A Preliminary Analysis. *Soil Tillage Res.* **2003**, *73*, 131–143. [CrossRef]
78. Huang, P.-T.; Patel, M.; Santagata, M.C.; Bobet, A. *Classification of Organic Soils*; Purdue University: West Lafayette, IN, USA, 2009. [CrossRef]
79. Panagos, P.; Meusburger, K.; Ballabio, C.; Borrelli, P.; Alewell, C. Soil Erodibility in Europe: A High-Resolution Dataset Based on LUCAS. *Sci. Total Environ.* **2014**, *479–480*, 189–200. [CrossRef] [PubMed]
80. Brakensiek, D.L.; Rawls, W.J.; Stephenson, G.R. Determining the Saturated Hydraulic Conductivity of a Soil Containing Rock Fragments. *Soil Sci. Soc. Am. J.* **1986**, *50*, 834–835. [CrossRef]
81. USDA. *National Soil Survey Handbook (NSSH). NRCS Soils*. Available online: https://www.nrcs.usda.gov/resources/guides-and-instructions/national-soil-survey-handbook (accessed on 6 August 2024).
82. Desmet, P.J.J.; Govers, G. Comment on Modelling Topographic Potential for Erosion and Deposition Using GIS. *Int. J. Geogr. Inf. Sci.* **1997**, *11*, 603–610. [CrossRef]
83. Smith, R.L. Extreme Value Analysis of Environmental Time Series: An Application to Trend Detection in Ground-Level Ozone. *Stat. Sci.* **1989**, *4*, 367–377. [CrossRef]
84. Haan, L.; Ferreira, A. *Extreme Value Theory: An Introduction*; Springer: Berlin/Heidelberg, Germany, 2006; Volume 21.
85. Makkonen, L.; Tikanmäki, M. An Improved Method of Extreme Value Analysis. *J. Hydrol. X* **2018**, *2*, 100012. [CrossRef]
86. Rossi, R.J. *Mathematical Statistics: An Introduction to Likelihood Based Inference*; John and Wiley and Sons: Hoboken, NJ, USA, 2018.
87. Yue, T.; Xie, Y.; Yin, S.; Yu, B.; Miao, C.; Wang, W. Effect of Time Resolution of Rainfall Measurements on the Erosivity Factor in the USLE in China. *Int. Soil Water Conserv. Res.* **2020**, *8*, 373–382. [CrossRef]
88. Alsumaiti, T.; Hussein, K.; Ghebreyesus, D.; Sharif, H. Performance of the CMORPH and GPM IMERG Products over the United Arab Emirates. *Remote Sens.* **2020**, *12*, 1426. [CrossRef]
89. Islam, M.A.; Yu, B.; Cartwright, N. Assessment and Comparison of Five Satellite Precipitation Products in Australia. *J. Hydrol.* **2020**, *590*, 125474. [CrossRef]
90. Pradhan, R.K.; Markonis, Y.; Vargas Godoy, M.R.; Villalba-Pradas, A.; Andreadis, K.M.; Nikolopoulos, E.I.; Papalexiou, S.M.; Rahim, A.; Tapiador, F.J.; Hanel, M. Review of GPM IMERG Performance: A Global Perspective. *Remote Sens. Environ.* **2022**, *268*, 112754. [CrossRef]
91. Panagos, P.; Borrelli, P.; Meusburger, K.; Yu, B.; Klik, A.; Lim, K.J.; Yang, J.E.; Ni, J.; Miao, C.; Chattopadhyay, N.; et al. Global Rainfall Erosivity Assessment Based on High-Temporal Resolution Rainfall Records. *Sci. Rep.* **2017**, *7*, 4175. [CrossRef]
92. Weng, X.; Zhang, B.; Zhu, J.; Wang, D.; Qiu, J. Assessing land use and climate change impacts on soil erosion caused by water in China. *Sustainability* **2023**, *15*, 7865. [CrossRef]
93. Montgomery, D.R. Soil Erosion and Agricultural Sustainability. *Proc. Natl. Acad. Sci. USA* **2007**, *104*, 13268–13272. [CrossRef] [PubMed]
94. Eekhout, J.P.; de Vente, J. Global impact of climate change on soil erosion and potential for adaptation through soil conservation. *Earth-Sci. Rev.* **2022**, *226*, 103921. [CrossRef]

95. Guerra, C.A.; Rosa, I.M.D.; Valentini, E.; Wolf, F.; Filipponi, F.; Karger, D.N.; Nguyen Xuan, A.; Mathieu, J.; Lavelle, P.; Eisenhauer, N. Global Vulnerability of Soil Ecosystems to Erosion. *Landsc. Ecol.* **2020**, *35*, 823–842. [CrossRef]
96. Oldeman, L.R.; Hakkeling, R.T.A.; Sombroek, W.G.; Batjes, N. *Global Assessment of Human-Induced Soil Degradation (GLASOD). World Map of the Status of Human-Induced Soil Degradation*; International Soil Reference and Information Centre: Wageningen, The Netherlands, 1991.
97. Meyer, R.; Zhang, W.; Kragh, S.J.; Andreasen, M.; Jensen, K.H.; Fensholt, R.; Stisen, S.; Looms, M.C. Exploring the combined use of SMAP and Sentinel-1 data for downscaling soil moisture beyond the 1 km scale. *Hydrol. Earth Syst. Sci.* **2022**, *26*, 3337–3357. [CrossRef]